Available online at www.sciencedirect.com

ScienceDirect

journal homepage: www.elsevier.com/locate/he

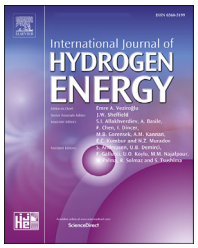

Compressive behaviour of thin catalyst layers. Part I - Experimental study

Ali Malekian [a], Sina Salari [a], Mickey Tam [b], Kevin Oldknow [c], Ned Djilali [d], Majid Bahrami [a,*]

[a] Laboratory for Alternative Energy Conversion (LAEC), School of Mechatronic Systems Engineering, Simon Fraser University, Surrey, BC, V3T 0A3, Canada
[b] Automotive Fuel Cell Cooperation, 9000 Glenlyon Parkway, Burnaby, BC, V5J 5J8, Canada
[c] Faculty of Applied Sciences, Simon Fraser University, Burnaby, BC, V5A 1S6, Canada
[d] Department of Mechanical Engineering and Institute for Integrated Energy Systems, University of Victoria, Victoria, BC, V8W 3P6, Canada

ARTICLE INFO

Article history:
Received 16 November 2018
Received in revised form
8 April 2019
Accepted 15 April 2019
Available online 4 June 2019

Keywords:
Catalyst layer
Compression
Porosity
Pressure
Mechanical properties
Young's modulus

ABSTRACT

In this study, the effect of compression is investigated experimentally on deformation and porosity of catalyst layers (CLs). Compression tests are performed on five CL samples with various microstructures using a thermomechanical analyzer and a custom-made machine Tuc-Ruc (Thickness under compression-Resistivity under compression). The results indicate that CLs have a linear behaviour with no plastic deformation at pressures less than 2 MPa even after 12 cycles. However, CLs showed plastic deformation, work hardening, and elastic shakedown under cyclic compression up to 5 MPa. In this pressure range, the material becomes stiffer and Young's modulus has increased by 50–113% after 8 loading cycles. Moreover, the material "settles down" after 6 cycles showing no further significant plastic deformation at higher pressures (up to 5 MPa). This behaviour suggests that CLs enter elastic shakedown region since after several cycles, plastic strain diminished, and they behave elastically afterwards. The compression tests on five samples yield Young's modulus of 30–45 MPa for pressures up to 2 MPa and Young's modulus of 37–70 MPa for pressures up to 5 MPa. The reason for slight change in Young's modulus is that the microstructure of CL changed, and the porosity decreased at higher pressures.

Introduction

The core of a Proton Exchange Membrane (PEM) fuel cell is the Membrane Electrode Assembly (MEA) which consists of several layers including a membrane, two catalyst layers (CLs), and two gas diffusion layers (GDL) [1,2]. During manufacturing and operation of a PEM fuel cell, the MEA goes through numerous load cycles and temperature/humidity changes. These induce hygrothermal stresses and lead to changes in microstructure, thermal, electrical and mechanical properties as well as cracks and delamination [3]. The hygrothermal stresses result in changes in membrane electrode assembly (MEA) properties which in turn impact the efficiency, life-time, and performance of the fuel cell [4–6]. As

* Corresponding author.
E-mail addresses: amalekia@sfu.ca (A. Malekian), mbahrami@sfu.ca (M. Bahrami).
https://doi.org/10.1016/j.ijhydene.2019.04.134

Nomenclature

V	Volume (mm^3)
W	Weight (N)
ρ	Density (kg/m^3)
t_0	Initial thickness (μm)
t_{new}	New thickness (μm)
Δt	Thickness change (μm)
ε_{new}	New porosity
ε_0	Initial porosity

Subscripts

b	Bulk
o	Octane
s	Solid
w	Water

such, the effects of varying mechanical loads (typically around 2 MPa in PEM fuel cell) on various porous layers of the MEA should be carefully studied to optimize efficiency, working conditions, and durability of fuel cells. In order to understand and optimize the performance of PEM fuel cell, material characterization, experimental studies, and modeling are needed to predict the behaviour of each layer. This research focuses on material characterization of CLs under compression to determine how CLs deform under compressive loads from bipolar plates combined with hygrothermal stresses. The first part of this work presented here focuses on the experimental study; model development and validation are presented in the accompanying paper [41].

Literature review

Many of the studies on CL and its microstructure are motivated by the need to decrease the cost of production, since CL is the most expensive layer of PEM fuel cells. Different methods were proposed, including: i) improvement by adding graphene [7,8], ii) platinum group metal-free (PGM-free) [9–11], and iii) low platinum loading (various methods) [2,12–17].

Most of studies that focused on mechanical properties of CLs have been done experimentally with a focus on crack formation. Changes in humidity, temperature, and pressure inside a PEM fuel cell stack also cause deformation and swelling of CL, and affect the porous structure and transport parameters [18,19]. Consequently, the performance and platinum utilization of a PEM fuel cell changes which is caused by deformation. A notable and comprehensive study on the mechanical properties of CL has been conducted by the Fuel Cell System Development Division of Toyota in Japan [5,20–24]. Kai et al. [5] studied crack formation of CL in tensile mode at various temperatures. They measured Young's modulus of the CL samples and membrane together and found that as temperature was increased, Young's modulus of the sample decreased. In another study by this group, Uchiyama et al. [22] studied the buckling and wrinkle formation of CL under humidity cycling. They calculated MEA stress under swelling using swelling ratio and Young's modulus and estimated critical stress for the buckling of the MEA. They used a flat surface made from polyimide film (PI) on GDL to prevent buckling and showed that by having a hole with bigger diameter on the polyimide film, the size of bulge and buckling increased which made part of the CL inactive. The effect of clearance height of the hole, which is the same as thickness of PI film, on top of CL was also investigated by the same group in a follow up study [21]. The results showed that for less than 25 μm clearance height, which correspond to local gap between layers, there was no crack on the CL even after 8500 humidity cycles.

Sassin et al. [25] recently reported on the influence of compressive stress on MEAs and found that the pore structure of the micro porous layer (MPL) is significantly altered at compressive stresses greater than about 0.9 MPa. However, the CL structure remained unaltered up to 1.4 MPa, the maximum compressive stress investigated.

Table 1 summarizes pertinent studies on mechanical properties of CL and their effect on PEM fuel cell performance. To the best of the authors' knowledge, there is no study on deformation of CLs under cyclic compression and no research has reported plastic deformation or work hardening of CLs under uniform compression. In this study, the behaviour of CLs under compression is investigated experimentally up to 5 MPa, which is complemented by development of a new effective medium model. The model is based on a geometrical "unit cell" that is presented in the Part II of this study [41].

Experimental study

Compression test setups

Two machines were used to perform compression tests on different CL samples; i) Thermomechanical Analyzer (TMA Q400EM, TA Instruments), and ii) a custom-made machine called Tuc-Ruc (Thickness Under Compression - Resistivity Under Compression).

The TMA compression tests were performed for pressures up to 2 MPa, the maximum allowed by this apparatus. The temperature of the TMA chamber can be controlled within ±1 °C in the range of −150 °C to 1000 °C. The maximum sample size is 26 mm in height (thickness) and 10 mm in width and length. A force ranging from 0.001 to 2 N can be applied on the samples using five different probes: expansion, macro-expansion, penetration, tension, and 3-point bending [26]. TMA measures displacement of the probe at various temperatures and can apply different types of loadings on the sample using a linear variable differential transformer (LVDT).

The thickness change of the sample was measured while the sample was subjected to linear force ramp with the rate of 0.1 N/min at 25 °C under compression probe. TMA resolution for displacement is less than 0.5 nm, which is small enough for measuring thickness change of CL samples. For all the performed tests, in order to ensure proper contact of the probe with the sample before compression, a preload force of 0.05 N was applied to the sample. A schematic of the sample holder and configuration of the probe in TMA Q400EM is shown in Fig. 1a.

Table 1 – Summary of available literature on mechanical properties of CLs.

Reference	Method	Contribution & findings
Sassin et al. [25]	Experimental	The CL structure is unaltered up to 1.4 MPa (confirmed by postmortem scanning electron microscopy and electrochemical evaluation)
Kai et al. [5]	Experimental	Investigated crack formation (in tensile) on CL that is coated on both sides of a membrane Measured Young's modulus of the sandwich samples Young's modulus of the sample decreases as temperature increases Crack initiation strain decreases as temperature increases
Uchiyama et al. [22]	Experimental	Buckling and wrinkle formation under humidity cycling Reported critical stress for buckling of CL Larger hole in the layer next to CL results in increase in the size of bulge, buckling, and crack formation Larger clamping force prevents the CL from wrinkling (no wrinkle at 200 N)
Uchiyama et al. [21]	Experimental	Effect of clearance height of the hole on top of CL is investigated No crack if clearance height is small (less than 25 μm) Plastic deformation of CL generates a bulge For large clearance height, swelling happens in in-plane direction so CL moves toward the clearance For small clearance height, swelling happens in through-plane direction and induces pressure on other layers
Kai et al. [24]	Experimental	Studied effect of carbon fibers on CL crack formation More space between carbon fibers results in earlier bulging Critical distance between fibers becomes narrower as temperature increases
Uchiyama et al. [23]	Experimental	Determined friction force between MPL and CL as a function of contact pressure At lower contact pressures, MEA deforms and wrinkles At higher contact pressures, bulging happens Static friction coefficient increases as the contact pressure increases

The Tuc-Ruc machine shown in Fig. 1b was designed by the Automotive Fuel Cell Cooperation (AFCC) to measure electrical resistivity and thickness under different pressures. This machine can apply up to 5 MPa pressure on a sample with maximum area of 2 cm^2. An initial pressure of 100 kPa was applied on the sample before performing the test to ensure the appropriate contact between sample and probe. The sample thickness was measured (using a Sony LT20A digital gauge) while it was subjected to loading and unloading cycles. Unlike the TMA which measures the thickness continuously, Tuc-Ruc only measures the thickness at the given pressures set by the user with accuracy of 1 μm. Dwelling time of 3 s was chosen for each pressure since shorter time was not possible. More dwelling times were not studied because it was suspected that longer dwelling times may introduce creep in the results.

CL compression

Substrate selection

Since the catalyst layer is not a stand-alone layer, it needs a substrate to be coated on for ex-situ measurements. These include measurements of thermal and electrical properties, diffusivity measurements as well as compression tests carried

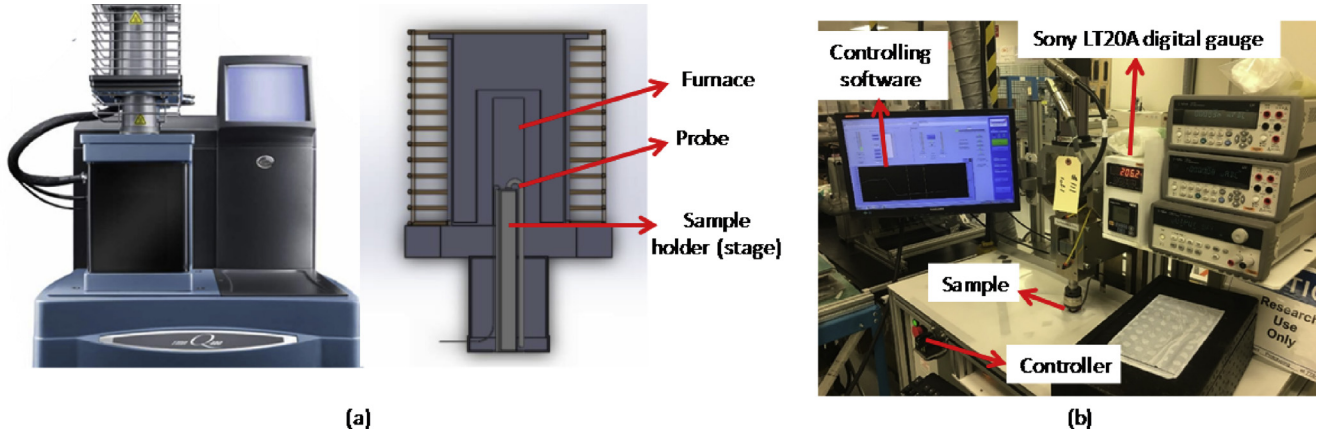

Fig. 1 – (a) TMA Q400EM schematic, (b) Tuc-Ruc (Thickness under compression - Resistivity under compression) apparatus used in this study.

out for this study. There were several candidates for CL substrate: ETFE (Ethylene tetrafluoroethylene) sheets, PTFE (Polytetrafluoroethylene) sheets, filter PTFE, aluminum foil, and silicon wafer. The most important criteria for selecting a substrate in compression tests are: i) the substrate should be sufficiently stiff to avoid significant deformation under compression; and ii) the substrate should be soft enough to allow easy sample cutting.

Aluminum foil was not a suitable candidate because it deforms and bends easily (resulting in a wavy surface). Silicon wafer is very stiff and hard to cut which means that the CL should be coated on silicon wafer after making silicon wafer small enough to fit in TMA machine. These limitations made silicon wafer and aluminum unsuitable candidates for compression tests.

Two other candidates, ETFE sheets and PTFE sheets, are similar. ETFE sheets are however more convenient for sample preparation and also their properties are known. Moreover, CLs coated on ETFE sheets yield a uniform thickness [27] which makes tests more reliable. Tests showed ETFE has adequate stiffness under compression. These characteristics made ETFE a suitable candidate for our compression tests.

Filter PTFE was used as substrate for CL diffusivity measurements in our previous study, where it was shown that the thickness of coated CL was uniform [28–30]. In this study, filter PTFE was also used as substrate of CL for compression tests up to 5 MPa using Tuc-Ruc machine. Although filter PTFE is a porous substrate, it worked well for these experiments because at higher pressures, all the void volumes within the substrate and between substrate and CL were compressed and crushed.

CL samples were compressed up to 5 MPa using both TMA and Tuc-Ruc. TMA was used to find compressive behaviour up to 2 MPa and Tuc-Ruc was used to obtain compression of CL for more than 2 MPa. Compressive behaviour of CLs from 0 to 5 MPa was then found by combining the results of both measurements from TMA and Tuc-Ruc.

CL porosity measurement

Porosity of each sample was measured using a densitometer at AFCC, which works similar to GDL porosity measurement that is done by Rashapov et al. [31]. This machine measures porosity using the Archimedes' principle. The difference between weight of an object in air (almost zero buoyancy force) and the weight in the liquid shows the volume of the displaced liquid. Since CL is hydrophobic on the surface and water cannot penetrate easily into the layer, it can be assumed that the volume of the layer is the same as the displaced volume of water. Hence, the bulk volume of the sample can be calculated using:

$$V_b = V_{\text{liquid}} = \frac{W_{\text{air}} - W_w}{g\rho_w} \tag{1}$$

where W_{air} and W_w are the measured weight in air and water, respectively, V_b is the bulk volume of the sample, g is the gravitational field, and ρ_w is density of water. To measure the porosity of the sample, the solid part of the volume needs to be determined. Since octane has low surface tension, it penetrates in almost all open pores of a porous sample. One can therefore measure weight of the sample in octane and find the porosity using Eqs. (2) and (3), in which W_o is the measured weight in octane, ρ_o is density of octane, and V_s is the solid volume of the porous layer.

$$V_s = \frac{W_{\text{air}} - W_o}{g\rho_o} \tag{2}$$

$$\varepsilon = 1 - \frac{V_s}{V_b} \tag{3}$$

Sample preparation

To coat CL on the substrate, various coating methods were evaluated including spraying, printing with Microfab and Fuji printers, Mayer bar (metering rod) coating, and decal transferring. As spraying and printing need a dilute ink to prevent nozzle clogging, high penetration of catalyst ink into the porous substrate was observed with these two methods. While having no penetration, decal transfer methods damage the substrate, as the transfer of the catalyst layer requires high compression and temperature (i.e. 15 bar and 150 °C). Mayer bar coating was chosen for this study as it can work with viscous ink (less penetration) and can be applied to delicate substrates. Mayer bar coats catalyst ink onto the substrate by spreading the ink with a rolling bar maintained at a specific distance above the surface, which determines the coating thickness. Moreover, the coated CL is uniform compared with printing based on our observations.

Five different CL samples were fabricated and tested in compression mode. These five designs had different ionomer to carbon weight ratios (I/C), porosities, and catalyst powder dry milling times. Standard ISO 13314:2011 [32] was followed to perform compression tests on CL samples. Since ETFE and filter PTFE were used as substrate, each sample was readily cut in sizes to fit in the machines and under the compression probe. Each CL design was tested three times to ensure the results were consistent; the average results are presented in this paper. The properties of the five samples are shown in Table 2. The porosity decreases by increase in dry milling time which is expected since dry milling crushes the agglomerates. All the designs were coated on both ETFE and filter PTFE. CLs coated on ETFE (substrate) were tested up to 2 MPa using TMA and CLs coated on filter PTFE (substrate) were tested up to 5 MPa using Tuc-Ruc to obtain the compressive behaviour of CL.

Cyclic compression tests

Compression tests using TMA (0–2 MPa). The thickness of each sample was measured by TMA right before exerting force on it to ensure accurate measurement and ensure that the sample handling had no considerable effect on the results

Table 2 – Properties of different CLs used in this study.

CL design number	I/C ratio	Dry Milling time (h)	Densitometer porosity (%)
Design 1	1.1	None	58.2 ± 2.0
Design 2	0.9	6	52.0 ± 1.6
Design 3	0.7	24	52.4 ± 2.1
Design 4	0.7	48	50.5 ± 1.9
Design 5	0.9	48	33.4 ± 1.3

(shown in Fig. 3b). To ensure the temperature of the sample was 25 °C, the machine was equilibrated at this temperature and 0.05 N force for 15 min. The deformation of ETFE was deducted from the results as well by finding the compression of ETFE at any given load. Compression tests were performed on all designs for 4 cycles to study the hysteresis effect and plastic deformation as well as the compressive behaviour of CLs up to 2 MPa. Only one of the designs was subjected to 12 cycles of compression tests in order to investigate the effect of the higher number of cycles.

Fig. 2a shows the pressure-strain behaviour of CL Design 1. This figure only shows the loading of the sample (and not the unloading part) to prevent the graph from appearing too complex. The unloading and loading curves were similar which suggested linear behaviour of the material in this region. The results revealed that the behaviour of CL did not change significantly over different cycles. The difference between cycles fell in the uncertainty range of the data which indicated that compressive behaviour in this design remained almost the same for each cycle. Moreover, no hysteresis effect and no plastic deformation were observed for the sample since the thickness of the sample did not change even after 12 cycles. Hence, the sample showed an elastic behaviour for this pressure range and one could calculate a Young's modulus from the experimental data. The measured Young's modulus for CL Design 1 is $E_{CL1} = 30.0 \pm 2.9\ MPa$. The relatively large uncertainty of Young's modulus is because of the difference between 12 cycles and the small thickness of the CL.

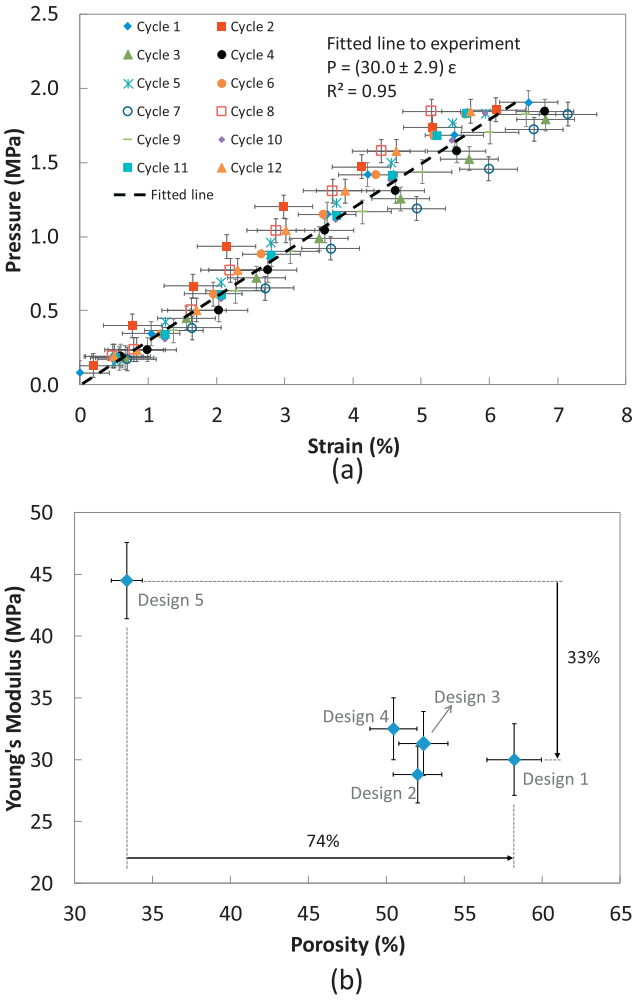

Fig. 2 – (a) Cyclic pressure vs strain of CL sample up to 2 MPa (Design 1), (b) Young's modulus of different CL Designs vs. porosity (up to 2 MPa).

Overall compressive behaviour and compression trend of all the samples are similar (CL Design 2 to 5 are shown in Fig. 6). All CL Designs were tested for 4 cycles and each test was repeated three times to ensure repeatability of the results. As mentioned, cyclic compression was continued up to 12 cycles for CL Design 1 and the behaviour did not change after the 4th cycle. All CL designs showed neither hysteresis nor plastic deformation during the compressive cycles. The results showed that the maximum strain for different designs at 2 MPa was between 5% and 7% which indicated that the samples were not rigid and that they deformed rather easily. However, CLs are generally more rigid than GDL since GDL's strain is about 15% at 2 MPa [33]. The results also revealed that Design 5 had the least deformation and the largest Young's modulus because of its lowest porosity.

The measured Young's modulus for each sample was in the range of 29–45 MPa. Fig. 2b shows the Young's modulus of all the CL samples as a function of porosity. As expected, the Young's modulus decreases as the porosity increases. This trend can be explained by noting that having more pores results in CL being a "softer" material. As it can be seen from Fig. 2b, CL Young's modulus decreased by 33% as the porosity was increased by 74% (CL Design 5 to CL Design 1). These results show that the CL porosity plays a key role in Young's modulus. Note that porosity in the samples is directly linked with the dry milling time in which the agglomerates are crushed; hence the porosity is decreased as dry milling time is increased. Hence, more dry milling time results in higher Young's modulus or stiffer CL.

Compression tests using Tuc-Ruc (0–5 MPa). In this study, the thickness of samples was measured at steps of 0.5 MPa starting from 0.5 MPa to 5 MPa. Because the resolution of thickness measurement of Tuc-Ruc machine is 1 μm, 10 stacks of CL coated on filter PTFE were prepared and tested, which also caused the uncertainty to decrease. Each CL sample was tested under compression for 8 cycles to investigate potential hysteresis effects and plastic deformation at higher pressures.

In the experiments using Tuc-Ruc machine, the first cycle was not considered in the data processing since the first cycle only closed the "gaps" between the layers in the stacks and compressed the filter PTFE (the porous substrate). Moreover, the results of the compression tests for less than 2 MPa was not accurate because at low pressures, the applied force was just enough to merely close the gaps. Therefore, the results for 2nd to 8th cycle are considered in this study. Deformation of a stack of 10 filter PTFE (without CL) was found at the same pressure steps; and the results were deducted from CL coated stack. Hence, the deformation of CL was obtained from these two sets of experiments.

Fig. 3a shows the thickness vs pressure for a stack of 10 CL Design 1 obtained from Tuc-Ruc machine for pressures more than 2 MPa. The results show that as the pressure increases, the thickness decreases, and the trend is linear for the

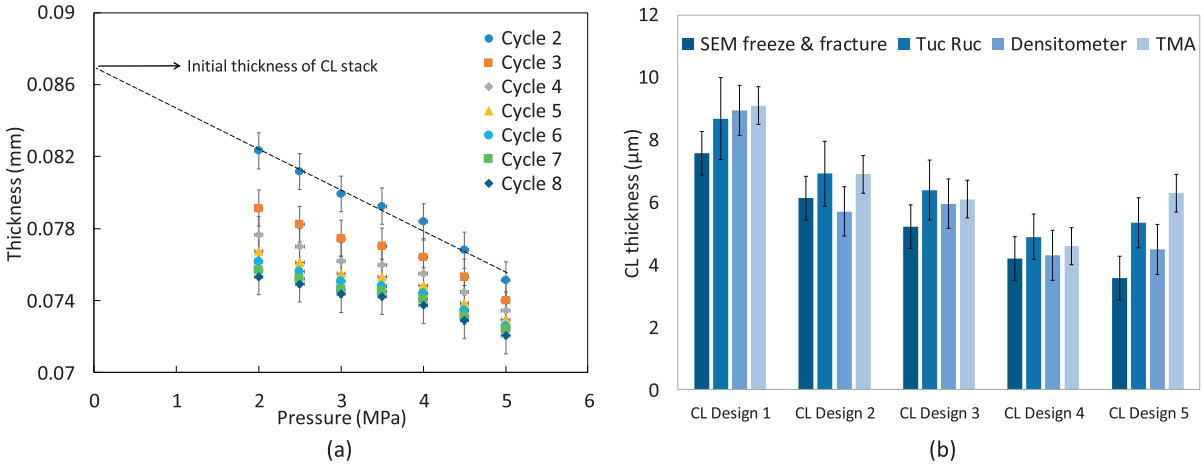

Fig. 3 – (a) Thickness vs pressure for a stack of CL Design1 from Tuc-Ruc (2–5 MPa), (b) Thickness of CL Designs measured using different methods (SEM [27,30], densitometer [27,30]).

thickness reduction. The figure also indicates that the thickness change for each cycle is different and the slope of thickness change is decreasing from cycle 2 to cycle 8. This increase in rigidity is observed because the sample pores are crushed, i.e. a decrease in porosity, hence the sample is harder to compress. Moreover, the CL shows permanent deformation as it is compressed up to 5 MPa. However, the material "settles down" after 6 cycles showing no further significant hysteresis effect and plastic deformation. Hence, CL is showing elastic shakedown in which the material goes through work hardening and after certain number of cycles, growth of residual strain diminishes, and the material behaves elastically for the following cycles.

The initial thickness of stack of 10 CL was estimated by extrapolating the line that goes through the 2nd cycle as shown in Fig. 3a. The measured thicknesses for all the designs using SEM [27,34], densitometer [27,34], TMA, and Tuc-Ruc are shown in Fig. 3b. This figure shows that thickness measured using different methods were within the uncertainty of results which indicates that the validity of Tuc-Ruc compression results.

To calculate the Young's modulus of CL for pressures more than 2 MPa, the applied pressure vs. strain data were used, see Fig. 4a for CL Design 1. As shown in Fig. 4a, the CL showed a plastic deformation from cycle 2 to cycle 8. Young's modulus of this region was calculated using the best-fit line to the experiment for each cycle as shown in Fig. 4. The slope of pressure-strain, or Young's modulus, was increased from the 2nd to 8th cycle which meant that the material became "stiffer" as it went through cycles. As the sample was compressed, more pores were closed, and more contact points were created in the CL, which resulted in a more rigid material and higher Young's modulus.

All the fabricated CL Designs showed similar behaviour at high pressures (up to 5 MPa). They showed permanent deformation on thickness and also work hardening which is caused by a decrease in porosity. As shown in Fig. 4a, the Young's modulus for the 2nd cycle was 37.6 MPa which increased to 80.2 MPa for 8th cycle (113% increase). However, the Young's modulus did not change significantly after the 6th cycle.

Fig. 4b shows the Young's modulus for different CL Designs from cycle 2 to 8. The results clearly indicate that Young's modulus of all the CL Designs increased as the samples were subjected to cyclic compression. As previously mentioned, this trend can be explained by the closure of pores (porosity decrease) and the creation of more contact points as the sample is compressed. Also, the Young's modulus of CL (at pressures more than 2 MPa) does not change appreciably beyond the 6th cycle, which indicates the material has equilibrated.

Table 3 shows the percentage change in Young's modulus from cycle 2 to cycle 8 for different Designs obtained from Fig. 4b. As it can be seen from Table 3, Young's modulus is increased by 113% for Design 1 and around 50% for Designs 2 to 5. Such trend is observed most likely because Design 1 had no dry milling, so it still had relatively larger pores and larger agglomerates and once it is compressed, more changes in its Young's modulus is observed. Also, the results suggest that for Design 2 (dry milling of 6 h), the change in Young's modulus is more than other Designs with more dry milling time. However, dry milling time more than 24 h did not have a significant effect on the change in Young's modulus.

Overall compression results (0–5 MPa). The experimental setups used in this study were chosen to complement each other. TMA covered the pressure range between 0 and 2 MPa and Tuc-Ruc covered the pressure range between 2 and 5 MPa. By combining the results of the two setups, one can obtain the compressive behaviour of CLs from 0 to 5 MPa.

Fig. 5 shows the pressure vs strain of CL Design 1 obtained from both TMA and Tuc-Ruc machine. The pressure vs strain slope changes slightly after 2 MPa for the first cycle (from E = 30 MPa to E = 37 MPa) and CL becomes stiffer at higher pressures. However, the behaviour for the following cycles (for higher pressures) is different; work hardening, and plastic deformation can be seen from the results. Since the compression results showed no plastic deformation from 0 to

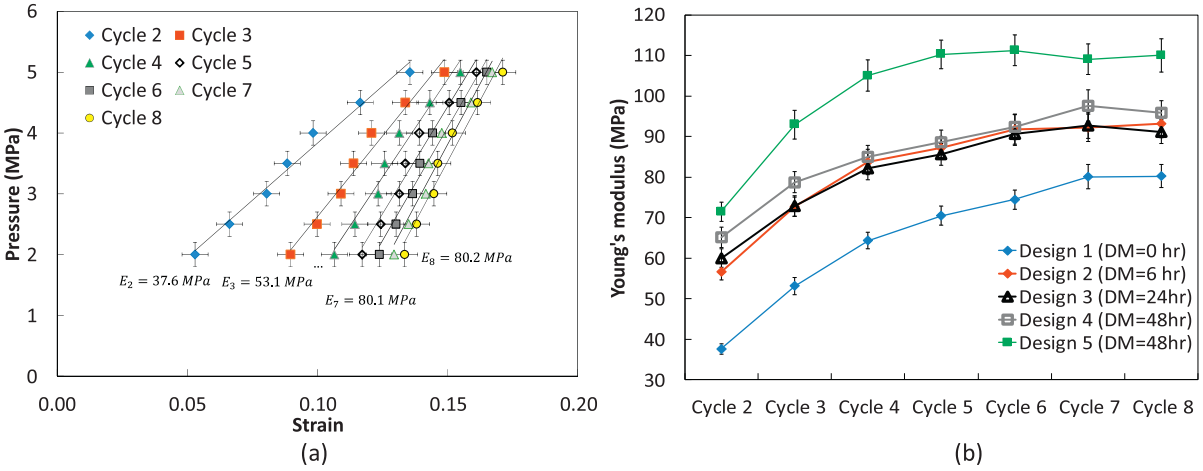

Fig. 4 – (a) Cyclic pressure-strain behaviour of CL sample up to 5 MPa (Design 1), (b) Young's modulus of CL samples for pressure up to 5 MPa under cyclic compression, DM: dry milling time in hours.

Table 3 – Percentage change of Young's modulus from cycle 2 to cycle 8 (2–5 MPa region) which is inversely proportional to dry milling time.

CL design number	Dry Milling time (h)	Percentage change of Young's modulus from cycle 2 to cycle 8
Design 1	None	113.2% ± 5.3%
Design 2	6	64.3% ± 4.3%
Design 3	24	52.1% ± 4.7%
Design 4	48	47.2% ± 3.9%
Design 5	48	53.9% ± 4.2%

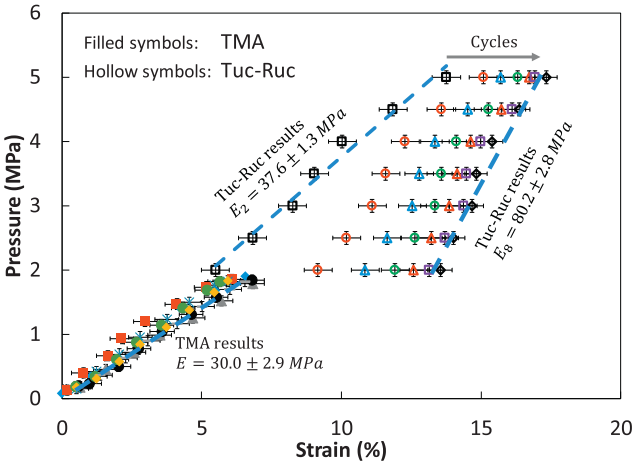

Fig. 5 – Pressure vs strain of CL Design 1 (0–5 MPa).

2 MPa and also showed work hardening effect from 0 to 5 MPa, the compressive behaviour of CL changed after 2 MPa. Other CL Designs also showed similar behaviour and showed plastic deformation after first cycle up to 5 MPa. Therefore, the compressive behaviour of CLs can be categorized into two pressure regions: i) pressures up to 2 MPa, ii) pressures up to 5 MPa. In the first region, the CL thickness decreases because of the elastic deformations occurring inside the CL. Also, it can be hypothesized that the CL microstructure remains intact as no plastic deformation is observed even after 12 cycles of loading (Fig. 2). Similar result was observed and published by Sassin et al. [25] as well. However, in the second region (pressures up to 5 MPa) the CL microstructure, and consequently the effective Young's modulus, is changed under cyclic compression as permanent deformation and work hardening are detected. Also, the CL showed more rigidity in second region (after the first cycle) as its porosity decreased and its microstructure changed. But the behaviour became consistent after 6 cycles.

Note that similar trends have been reported for other porous materials as well [33,35]. In a separate study, Shen [36] found that as the indentation in CL increases, the Young's modulus also increases. This is consistent with our results since by applying more pressure, CL showed more rigid behaviour. The hardening effect happens in random porous materials because of decrease in porosity and creation of more contact nodes as compression increases. Moreover, the thickness vs pressure results for Tuc-Ruc apparatus as shown in Fig. 3 shows the initial thickness of the CL stack which also suggest the validity of the results.

Other CL Designs also showed a similar behaviour under cyclic compression. The results of CL compression are shown in Fig. 6 for CL Designs 2, 3, 4, and 5. They all showed a slight change in Young's modulus and plastic deformation after 2 MPa pressure for the first cycle. A reason for this slight increase in Young's modulus might be the decrease of void volume inside CL (porosity decreases) which results in more rigidity of this porous layer. Also, CL showed work hardening and plastic deformation for the following cycles by applying 5 MPa cyclic compressionp. In other words, CL had "elastic-plastic" behaviour under cyclic compression. The onset of the plastic deformation was approximately 2 MPa; however, this onset pressure can also be more than 2 MPa. This means that the yield pressure for catalyst layer is around 2 MPa (somewhere between 2 and 5 MPa) beyond which it shows plastic deformation and work hardening because of the change in microstructure. As found by Sassin et al. [25], no plastic

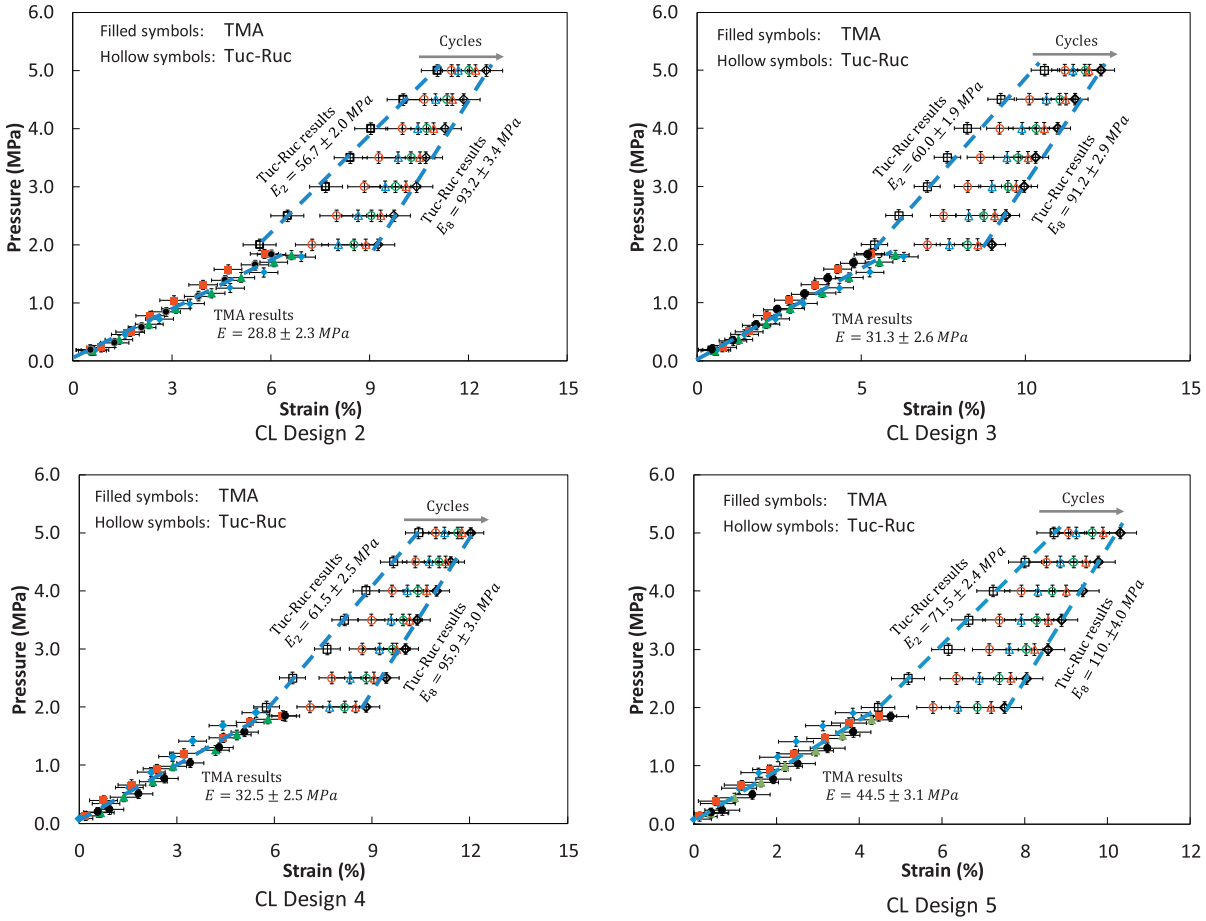

Fig. 6 – Pressure vs strain of different CL designs (0–5 MPa).

deformation occurs at pressures lower than 1.4 MPa which is consistent with the results in this paper. Unlike conventional materials which become softer after their yield pressure, CL hardens due to its porous nature.

The pressure-strain curves of CL samples showed that by applying 2 MPa pressure on CL, this layer behaved as a linear elastic material. However, by increasing the pressure up to 5 MPa, CL showed elastic shakedown behaviour. This means that CL went through work hardening and plastic deformation during cyclic load but after certain number of cycles, the growth of residual strain gradually decreased and diminished. This behaviour also showed that the yield pressure (or the boundary of elastic and shakedown behaviour) for CL is between 2 and 5 MPa. It is interesting that CL, which is a porous thin layer made from carbon particle, ionomer, and Pt particles, is showing shakedown behaviour. This behaviour is seen in many conventional engineering structures and materials such as granular materials, steel, rail surfaces, etc. [37–40]. In conclusion, a composite porous thin layer (CL) is behaving similar to conventional engineering structures so Bree's interaction diagram can be determined. However, unlike typical structures, CL will have three axes: pressure, temperature, and humidity because both temperature and humidity have considerable effect on mechanical properties of CL. In this work, only pressure is studied, and more research is needed to complete Bree's interaction diagram for CL.

As shown in Figs. 5 and 6, the strains (at 5 MPa for the first cycle) of different CL Designs are between 9% and 14%. CL Design 1 that had the highest porosity has the highest maximum strain at 5 MPa and the Design 5 with the lowest porosity has the least maximum strain. These results show that as porosity of CL increases, it becomes softer and easier to compress. It also shows that compression has a more pronounced effect on deformation of CL with higher porosity.

Porosity is a key factor to find other properties of CLs such as thermal and electrical conductivity and gas diffusivity that are also dependent on porosity and mechanical pressure. Having the pressure vs strain data for each CL design and knowing the initial porosity of the CLs, one can determine the porosity of the samples as a function of applied pressure. The porosity at any given strain can be found using Eq. (4), where ε_{new} and ε_0 are the new and initial porosities, respectively, t_{new} and t_0 are new and initial thicknesses, respectively, Δt is the change in thickness, and $\Delta t / t_0$ is strain.

$$\varepsilon_{new} = 1 - \frac{t_0}{t_{new}}(1 - \varepsilon_0) \quad \text{or} \quad \varepsilon_{new} = 1 - \frac{1}{1 - \frac{\Delta t}{t_0}}(1 - \varepsilon_0) \tag{4}$$

Fig. 7 shows the strain vs pressure (first vertical axis) and porosity vs pressure (second vertical axis) for CL Design 1. In

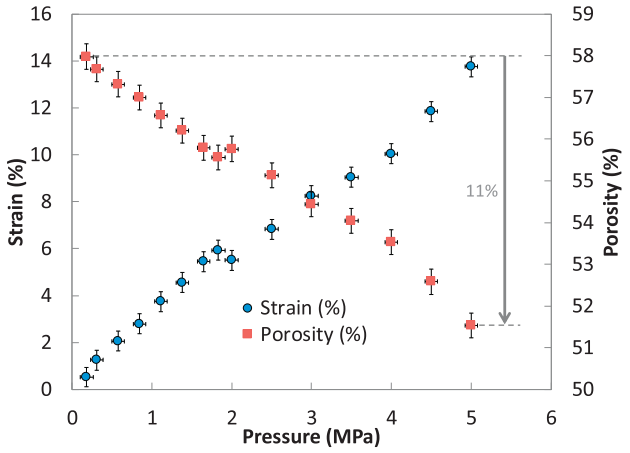

Fig. 7 – Pressure vs porosity and strain of CL Design 1.

this figure, only one loading cycle of the results of TMA is shown to not clutter the figure and also the first loading of Tuc-Ruc results are shown. One can conclude the following: i) as the compressive load is increased, the strain increases and porosity decreases; ii) the trend for porosity decrease contains two almost linear regions in the considered pressure range; iii) the initial porosity of Design 1 was 58% which is decreased to 51% after compression of 14%. This change in porosity is important to study some other properties of CL under compression, such as diffusivity.

Figs. 7 and 8 show the pressure vs porosity and strain for CL Designs 1 to 5. The behaviour and trend of CL strain and porosity vs pressure is similar for all the Designs. The mentioned figures show that strain increases, and porosity decreases as the compressive load is increased. The porosity decreases in two almost linear regions which are from 0 to 2 MPa and from 2 MPa to 5 MPa. The porosity reduction of each sample is dependent on the initial porosity and strain at any given pressure. As shown in Figs. 7 and 8, the reduction in porosity of different CL Designs are between 10 and 19%.

Porosity reduction of all CL samples is also shown in Fig. 9. The results show the porosity before compression, at 2 MPa pressure, and after the first load cycle of 5 MPa pressure. The figure clearly shows the reduction in porosity after compression; the percentage change of porosity after 5 MPa pressure is written next to each design. The following can be concluded: i) porosity reduction for each Design is different; ii) porosity

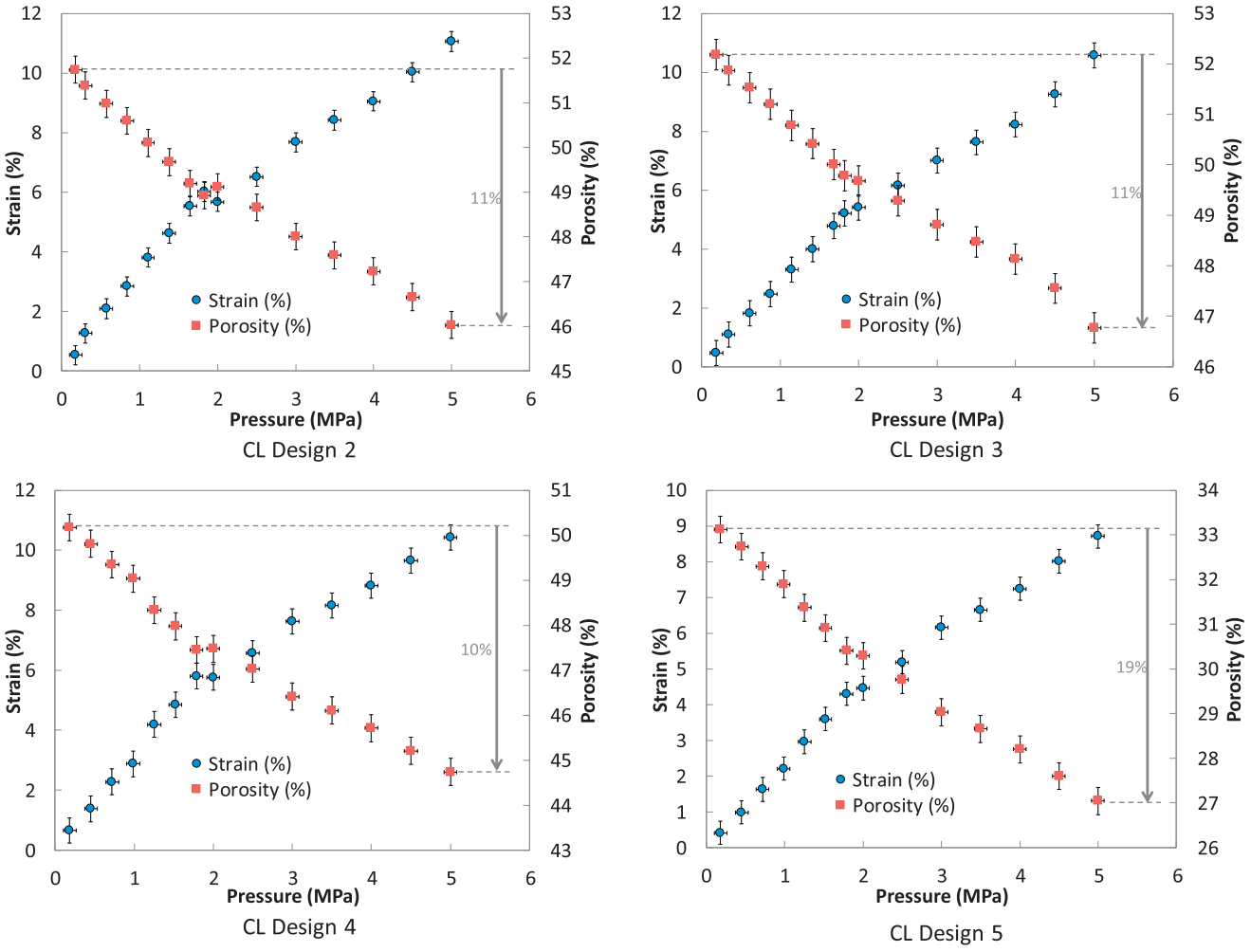

Fig. 8 – Pressure vs porosity and strain of different CL Designs.

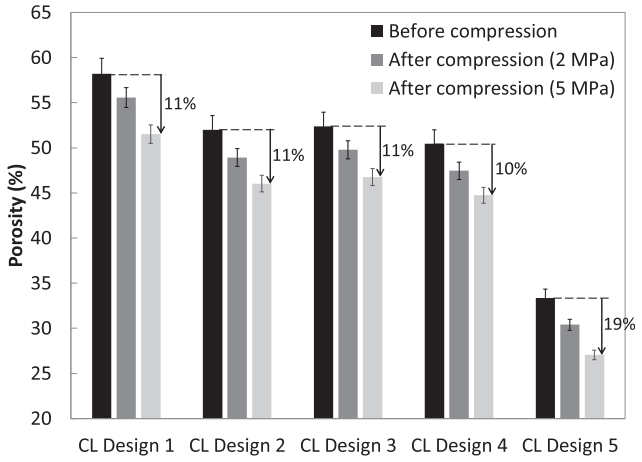

Fig. 9 – Porosity of CL designs before and after compression.

reduction is the highest for CL Design 5, which has the lowest initial porosity, and other CL Designs showed similar percentage change in porosity; iii) compression has a more pronounced effect on percentage change in porosity of samples with lower initial porosity (e.g. CL Design 5 with 33% initial porosity shows a 19% change in porosity after compression).

Conclusions

In this study, a new procedure was developed to measure mechanical deformation of CL coated on a substrate and their porosity was calculated over a range of pressures. Five CL designs were coated on ETFE and filter PTFE using Mayer bar and their thicknesses were measured using TMA and Tuc-Ruc right before each compression test to minimize the uncertainty. The initial porosity of the CL samples was measured using a custom-made densitometer. Five CL Designs with various properties such as ionomer to carbon weight ratio, porosity, and dry milling time were tested. Results showed that CLs have elastic behaviour for pressures lower than 2 MPa, which means that the microstructure of CL does not change significantly, and no plastic deformation happens even after 12 compression cycles. However, the behaviour changes when 5 MPa pressure is applied; CL showed a slight change in Young's modulus after 2 MPa for the first cycle and also Young's modulus increased as the number of cycles increased. Plastic deformation and work hardening effect shows that the microstructure of CL is changed by applying cyclic 5 MPa pressure. Results showed that CLs had elastic-plastic behaviour with yield pressure of around 2 MPa, beyond which CL became more rigid and its microstructure changed. Experimental results suggested that CL compressive behaviour had two regions: i) pressures up to 2 MPa, ii) pressures up to 5 MPa. In the first region, the behaviour is linear elastic with no permanent (plastic) deformation or hysteresis even after 12 loading cycles. It is found that higher porosity designs yield lower Young's modulus for this region (up to 2 MPa) as well. However, by applying 5 MPa cyclic pressure, CL showed plastic deformation and work hardening which are indications for change in microstructure. CL also entered elastic shakedown region since it showed plastic deformation for several cycles and it diminished after that, which means the boundary between elastic and shakedown behaviour is 2–5 MPa. Also, Young's modulus of CL (for the first cycle up to 5 MPa) increased slightly after 2 MPa since the porosity of the layer decreased and more contact points were created within CLs. Moreover, the effective Young's modulus (for pressures up to 5 MPa) was found to increase by cycles because of the decrease in porosity (i.e. sample pores got crushed at high pressure). In addition, the material showed elastic shakedown since no significant change was seen on CL compressive behaviour after 6 cycles at high pressures.

Acknowledgements

This research was supported by funding from the Natural Sciences and Engineering Research Council of Canada Collaborative Research and Development (Grant No. CRDPJ 452170-13) and Automotive Fuel Cell Corporation (AFCC), Canada. AFCC Structure, Properties & Performance Research Division is also acknowledged for their technical support.

REFERENCES

[1] Litster S, McLean G. PEM fuel cell electrodes. J Power Sources 2004;130:61–76. https://doi.org/10.1016/j.jpowsour.2003.12.055.
[2] Secanell M, Karan K, Suleman A, Djilali N. Optimal design of ultralow-platinum PEMFC anode electrodes. J Electrochem Soc 2008;155:B125. https://doi.org/10.1149/1.2806171.
[3] Banan R, Zu J, Bazylak A. Humidity and temperature cycling effects on cracks and delaminations in PEMFCs. Fuel Cells 2015;15:327–36. https://doi.org/10.1002/fuce.201400118.
[4] Tang Y, Santare MH, Karlsson AM, Cleghorn S, Johnson WB. Stresses in Proton Exchange membranes due to hygro-thermal loading. J Fuel Cell Sci Technol 2006;3:119. https://doi.org/10.1115/1.2173666.
[5] Kai Y, Kitayama Y, Omiya M, Uchiyama T, Kato M. Crack formation on membrane electrode assembly (MEA) under static and cyclic loadings. J Fuel Cell Sci Technol 2012;10:143. https://doi.org/10.1115/FuelCell2012-91164.
[6] Kusoglu A, Karlsson AM, Santare MH, Cleghorn S, Johnson WB. Mechanical response of fuel cell membranes subjected to a hygro-thermal cycle. J Power Sources 2006;161:987–96. https://doi.org/10.1016/j.jpowsour.2006.05.020.
[7] Zhou X, Qiao J, Yang L, Zhang J. A review of graphene-based nanostructural materials for both catalyst supports and metal-free catalysts in PEM fuel cell oxygen reduction reactions. Adv Energy Mater 2014;4:1301523. https://doi.org/10.1002/aenm.201301523. n/a.
[8] Peng H, Mo Z, Liao S, Liang H, Yang L, Luo F, et al. High performance Fe- and N- doped carbon catalyst with graphene structure for oxygen reduction. Sci Rep 2013;3:1765. https://doi.org/10.1038/srep01765.
[9] Serov A, Workman MJ, Artyushkova K, Atanassov P, McCool G, McKinney S, et al. Highly stable precious metal-free cathode catalyst for fuel cell application. J Power Sources

2016;327:557–64. https://doi.org/10.1016/J.JPOWSOUR.2016.07.087.
[10] Serov A, Shum AD, Xiao X, de Andrade V, Artyushkova K, Zenyuk IV, et al. Nano-structured platinum group metal-free catalysts and their integration in fuel cell electrode architectures. Appl Catal B Environ 2018;237:1139–47. https://doi.org/10.1016/J.APCATB.2017.08.067.
[11] Zhang H, Osgood H, Xie X, Shao Y, Wu G. Engineering nanostructures of PGM-free oxygen-reduction catalysts using metal-organic frameworks. Nanomater Energy 2017;31:331–50. https://doi.org/10.1016/J.NANOEN.2016.11.033.
[12] Owejan JP, Owejan JE, Gu W. Impact of platinum loading and catalyst layer structure on PEMFC performance. J Electrochem Soc 2013;160:F824–33. https://doi.org/10.1149/2.072308jes.
[13] Çögenli MS, Mukerjee S, Yurtcan AB. Membrane electrode assembly with ultra low platinum loading for cathode electrode of PEM fuel cell by using sputter deposition. Fuel Cells 2015;15:288–97. https://doi.org/10.1002/fuce.201400062.
[14] Kongkanand A, Subramanian NP, Yu Y, Liu Z, Igarashi H, Muller DA. Achieving high-power PEM fuel cell performance with an ultralow-Pt-content core–shell catalyst. ACS Catal 2016;6:1578–83. https://doi.org/10.1021/acscatal.5b02819.
[15] Breitwieser M, Klingele M, Britton B, Holdcroft S, Zengerle R, Thiele S. Improved Pt-utilization efficiency of low Pt-loading PEM fuel cell electrodes using direct membrane deposition. Electrochem Commun 2015;60:168–71. https://doi.org/10.1016/j.elecom.2015.09.006.
[16] Xie S, Choi S-I, Lu N, Roling LT, Herron JA, Zhang L, et al. Atomic layer-by-layer deposition of Pt on Pd nanocubes for catalysts with enhanced activity and durability toward oxygen reduction. Nano Lett 2014;14:3570–6. https://doi.org/10.1021/nl501205j.
[17] Martin S, Garcia-Ybarra PL, Castillo JL. Electrospray deposition of catalyst layers with ultra-low Pt loadings for PEM fuel cells cathodes. J Power Sources 2010;195:2443–9. https://doi.org/10.1016/j.jpowsour.2009.11.092.
[18] Lange KJ, Sui PC, Djilali N. Determination of effective transport properties in a PEMFC catalyst layer using different reconstruction algorithms. J Power Sources 2012;208:354–65. https://doi.org/10.1016/j.jpowsour.2011.11.001.
[19] Singh R, Akhgar AR, Sui PC, Lange KJ, Djilali N. Dual-beam FIB/SEM characterization, statistical reconstruction, and pore scale modeling of a PEMFC catalyst layer. J Electrochem Soc 2014;161:F415–24. https://doi.org/10.1149/2.036404jes.
[20] Uchiyama T, Kato M, Ikogi Y, Yoshida T. Mechanical degradation mechanism of membrane electrode assemblies in buckling test under humidity cycles. J Fuel Cell Sci Technol 2012;9:061005. https://doi.org/10.1115/1.4007814.
[21] Uchiyama T, Kumei H, Yoshida T. Catalyst layer cracks by buckling deformation of membrane electrode assemblies under humidity cycles and mitigation methods. J Power Sources 2013;238:403–12. https://doi.org/10.1016/j.jpowsour.2013.04.026.
[22] Uchiyama T, Kato M, Yoshida T. Buckling deformation of polymer electrolyte membrane and membrane electrode assembly under humidity cycles. J Power Sources 2012;206:37–46. https://doi.org/10.1016/j.jpowsour.2012.01.073.
[23] Uchiyama T, Kumei H, Yoshida T, Ishihara K. Static friction force between catalyst layer and micro porous layer and its effect on deformations of membrane electrode assemblies under swelling. J Power Sources 2014;272:522–30. https://doi.org/10.1016/j.jpowsour.2014.08.103.
[24] Kai Y, Kitayama Y, Omiya M, Uchiyama T, Kumei H. In situ observation of deformation behavior of membrane electrode assembly under humidity cycles. J Fuel Cell Sci Technol 2014;11:051006. https://doi.org/10.1115/1.4028155.
[25] Sassin MB, Garsany Y, Gould BD, Swider-Lyons K. Impact of compressive stress on MEA pore structure and its consequence on PEMFC performance. J Electrochem Soc 2016;163:F808–15. https://doi.org/10.1149/2.0291608jes.
[26] Waguespack L. TA Instruments. 2013. p. 1–21.
[27] Ahadi M, Tam M, Saha MS, Stumper J, Bahrami M. Thermal conductivity of catalyst layer of polymer electrolyte membrane fuel cells: Part 1 – experimental study. J Power Sources 2017;354:207–14. https://doi.org/10.1016/j.jpowsour.2017.02.016.
[28] Salari S, McCague C, Tam M, Saha M, Stumper J, Bahrami M. Accurate ex-situ measurements of PEM fuel cells catalyst layer dry diffusivity. ECS Trans 2015;69:419–29.
[29] Salari S, Stumper J, Bahrami M. Direct measurement and modeling relative gas diffusivity of PEMFC catalyst layers: the effect of ionomer to carbon ratio, operating temperature, porosity, and pore size distribution. Int J Hydrogen Energy 2018;43:16704–18. https://doi.org/10.1016/j.ijhydene.2018.07.035.
[30] Salari S. Gas diffusion in thin porous catalyst layers of PEM fuel cells. Simon Fraser University; 2018.
[31] Rashapov RR, Unno J, Gostick JT. Characterization of PEMFC gas diffusion layer porosity. J Electrochem Soc 2015;162:F603–12. https://doi.org/10.1149/2.0921506jes.
[32] Standard I. ISO 13314 Mechanical testing of metals, ductility testing, compression test for porous and cellular metals. 2011. p. 1–7. Ref. Number ISO. 13314, www.iso.org.
[33] Malekian A, McCague C, Salari S, Djilali N, Bahrami M. Compression of pem fuel cell gas diffusion layers: analytical model and experimental validation. In: 27th int. Symp. Transp. Phenom.; 2016. Honolulu.
[34] Salari S, Stumper J, Bahrami M. Through plane gas diffusion of catalyst layer of PEMFC: bimodal unit cell modeling. In: 27th inernational symp. Transp. Phenom.; 2016. Honolulu.
[35] Hoseini A, Malekian A, Bahrami M. Deformation and thermal resistance study of aerogel blanket insulation material under uniaxial compression. Energy Build 2016;130:228–37. https://doi.org/10.1016/j.enbuild.2016.08.053.
[36] Shen Y. Mechanical degradation of membrane electrode assemblies in Proton Exchange membrane fuel cells. University of Waterloo; 2017.
[37] Bidiville A, Favero M, Stadelmann P, Mischler S. Effect of surface chemistry on the mechanical response of metals in sliding tribocorrosion systems. Wear 2007;263:207–17. https://doi.org/10.1016/j.wear.2007.01.066.
[38] Stein E, Zhang G, König JA. Shakedown with nonlinear strain-hardening including structural computation using finite element method. Int J Plast 1992;8:1–31. https://doi.org/10.1016/0749-6419(92)90036-C.
[39] Werkmeister S, Dawson A, Wellner F. Permanent deformation behavior of granular materials and the shakedown concept. Transport Res Rec 2005;1757:75–81. https://doi.org/10.3141/1757-09.
[40] Ponter ARS, Hearle AD, Johnson KL. Application of the kinematical shakedown theorem to rolling and sliding point contacts. J Mech Phys Solids 1985;33:339–62. https://doi.org/10.1016/0022-5096(85)90033-X.
[41] Malekian A, Salari S, Tam M, Oldknow K, Djilali N, Bahrami Majid. Compressive behaviour of thin catalyst layers. Part II - Experimental study. Int J Hydrogen Energy 2018. https://doi.org/10.1016/j.ijhydene.2019.04.135.